Neuroradiology
https://doi.org/10.1007/s00234-022-02950-9

GUIDELINES

Guidelines for magnetic resonance imaging in pediatric head and neck pathologies: a multicentre international consensus paper

Felice D'Arco[1,2] · Livja Mertiri[1,3] · Pim de Graaf[4] · Bert De Foer[5] · Katarina S. Popovič[6] · Maria I. Argyropoulou[7] · Kshitij Mankad[1] · Hervé J. Brisse[8,9] · Amy Juliano[10] · Mariasavina Severino[11] · Sophie Van Cauter[12,13] · Mai-Lan Ho[14,15] · Caroline D. Robson[16] · Ata Siddiqui[2,17] · Steve Connor[2,17,18] · Sotirios Bisdas[19,20] · on behalf of the Consensus for Magnetic Resonance Protocols Study (COMPS) Group

Received: 16 February 2022 / Accepted: 5 April 2022

Abstract

The use of standardized imaging protocols is paramount in order to facilitate comparable, reproducible images and, consequently, to optimize patient care. Standardized MR protocols are lacking when studying head and neck pathologies in the pediatric population. We propose an international, multicenter consensus paper focused on providing the best combination of acquisition time/technical requirements and image quality. Distinct protocols for different regions of the head and neck and, in some cases, for specific pathologies or clinical indications are recommended. This white paper is endorsed by several international scientific societies and it is the result of discussion, in consensus, among experts in pediatric head and neck imaging.

Keywords Head and neck images · Pediatric neuroradiology · Magnetic resonance imaging · Standardized protocols · Guidelines

FD'A and LM contributed equally to the paper.

✉ Livja Mertiri
livja.mertiri16@gmail.com

Felice D'Arco
felice.d'arco@gosh.nhs.uk

Pim de Graaf
p.degraaf@amsterdamumc.nl

Bert De Foer
bert.defoer@gza.be

Katarina S. Popovič
katarina.surlan@kclj.si

Maria I. Argyropoulou
margyrop@uoi.gr

Kshitij Mankad
kshitij.mankad@gosh.nhs.uk

Hervé J. Brisse
herve.brisse@curie.fr

Amy Juliano
amy_juliano@meei.harvard.edu

Mariasavina Severino
mariasavinaseverino@gaslini.org

Sophie Van Cauter
sofie.vancauter@zol.be

Mai-Lan Ho
mailanho@gmail.com

Caroline D. Robson
Caroline.Robson@childrens.harvard.edu

Ata Siddiqui
ata.siddiqui@gstt.nhs.uk

Steve Connor
steve.connor@kcl.ac.uk

Sotirios Bisdas
s.bisdas@ucl.ac.uk

[1] Radiology Department, Great Ormond Street Hospital for Children, London, UK

[2] Radiology Department, Guy's and St Thomas' NHS Foundation Trust, London, UK

[3] Faculty of Medicine and Dentistry, Sapienza University of Rome, Rome, Italy

[4] Department of Radiology and Nuclear Medicine, Cancer Center Amsterdam, Amsterdam UMC, Vrije Universiteit Amsterdam, Amsterdam, The Netherlands

[5] Radiology Department, GZA Hospitals, Antwerp, Belgium

Published online: 23 April 2022

Abbreviations

ADC	Apparent diffusion coefficient (map from the DWI)
ASL	Arterial spin labeling
AVF	Arterio-venous fistula
AVM	Arterio-venous malformation
CBCT	Cone beam CT
CHL	Conductive hearing loss
CI	Cochlear implant
CISS	Constructive interference in steady state
CNS	Central nervous system
COMPS	Consensus for Magnetic Resonance Protocols Study Group
CSF	Cerebrospinal fluid
CT	Computed tomography
DCE	Dynamic contrast enhancement
DWI	Diffusion weighted imaging
EPI	Echo planar imaging
FIESTA-C	Fast imaging employing steady-state acquisition with constructive interference in steady state
FLAIR	Fluid-attenuated inversion recovery
FS	Fat suppression
Gd	Gadolinium
GRE	Gradient recalled echo
IAC	Internal auditory canal
LAVA	Liver acquisition with volume acceleration
LCH	Langerhans cell histiocytosis
MDCT	Multidetector CT
MPR	Multiplanar reconstruction
MPRAGE	Magnetization prepared rapid gradient echo
MRA	Magnetic resonance angiography
MRI	Magnetic resonance imaging
MRV	Magnetic resonance venography (venous TOF or venous phase contrast MR)
PNS	Perineural tumor spread
RB	Retinoblastoma
RF	Radiofrequency
RMS	Rhabdomyosarcoma
SL	Slice thickness
SNHL	Sensorineural hearing loss
SPACE	Sampling perfection with application-optimized contrasts by using flip angle evolution
STIR	Short tau inversion recovery
SWI	Susceptibility weighted imaging
TrueFISP	True fast imaging with steady state precession
T	Tesla
TOF	Time of flight
THRIVE	T1 high-resolution isotropic volume excitation
TSE	Turbo spin echo
US	Ultrasound
VIBE	Volumetric interpolated breath-hold examination
VISTA	Volume isotropic turbo spin echo acquisition
WI	Weighted image

[6] Neuroradiology Department, Clinical Institute of Radiology, University Medical Center Ljubljana, Zaloška 7, 1000 Ljubljana, Slovenia

[7] Department of Clinical Radiology and Imaging, Medical School, University of Ioannina, Ioannina, Greece

[8] Imaging Department, Institut Curie, Paris, France

[9] Institut Curie, Paris Sciences Et Lettres (PSL) Research University, Paris, France

[10] Department of Radiology, Massachusetts Eye and Ear, Harvard Medical School, Boston, MA, USA

[11] Neuroradiology Unit, IRCCS Istituto Giannina Gaslini, Genoa, Italy

[12] Department of Medical Imaging, Ziekenhuis Oost-Limburg, Genk, Belgium

[13] Faculty of Medicine and Life Sciences, Hasselt University, Hasselt, Belgium

[14] Nationwide Children's Hospital, Columbus, OH, USA

[15] The Ohio State University, Columbus, OH, USA

[16] Department of Radiology, Boston Children's Hospital, Harvard Medical School, Boston, MA, USA

[17] Department of Neuroradiology, King's College Hospital NHS Foundation Trust, London, UK

[18] School of Biomedical Engineering and Imaging Sciences, St Thomas' Hospital, King's College, London, UK

[19] Lysholm Department of Neuroradiology, The National Hospital for Neurology & Neurosurgery, University College London Hospitals NHS Foundation Trust, London, UK

[20] Department of Brain Repair and Rehabilitation, UCL Queen Square Institute of Neurology, London, UK

Introduction

The use of standardized imaging protocols is fundamental in order to facilitate comparable, reproducible images and, consequently, to help standardize patient care [1].

MRI offers many advantages in comparison to CT in terms of contrast resolution and superior soft tissue detail [2]; however, precise sequence selection needs to be tailored for the study of different body regions [3].

When studying head and neck pathologies, it is very important to use sequences and hardware (combination of MRI field-strength and coil set-up) that allow definition and characterization of various pathological processes, and to distinguish these processes from normal tissue (in particular surrounding fat and muscles) and developmental variants [4].

In addition, the pediatric population is affected by diseases that differ from adults and has specific issues to be addressed (such as, myelination when imaging the brain, movement artifacts, right-sized field of view, necessity of sedation or general anesthesia, etc.). Therefore, it is essential to optimize MR protocols not only for the various body regions studied, but also tailored to children [2].

The aim of this paper is to provide standardized, disease/region–specific MR protocols for assessment of pediatric head and neck pathologies.

Methods

We first assessed the variability of head and neck protocols across institutions in Europe and North America, and then provided a consensus based on the opinion of the members of different European radiology societies and specific committees.

A first paper version was drafted by the co-first authors (FD'A and LM) and the last author (SB) after agreeing on the paper's main paragraphs and a search of the relevant literature. The draft was subsequently circulated among the co-authors and collaborators of the COMPS group (which includes pediatric radiologists, neuroradiologists, radiologists with special interest in head and neck imaging, MR physicists, oncologists, surgeons and radiographers) and representatives of the endorsing scientific societies. After all comments were received, they were either integrated in the revised manuscript or, when discordant opinions were present, they were resolved by consensus. The final manuscript was again shared with the group.

Endorsements

This consensus statement started as an initiative of the British Pediatric Neuroimaging Group (BPNG) and of the Head and Neck Committee of the European Society of NeuroRadiology (ESNR). It is endorsed by the European Society of NeuroRadiology (ESNR), the British Pediatric Neuroimaging Group (BPNG), the British Society of Head and Neck Imaging (BSHNI), the European Society of Head and Neck Radiology (ESHNR), the Italian Association of NeuroRadiology (AINR), the European Retinoblastoma Imaging Collaboration (ERIC) and the European Society of Pediatric Radiology (ESPR).

Surveys

We created a series of surveys which were sent to members of the ESNR, BPNG, ESPR, BSHNI, ESHNR and AINR in order to gather information on what protocols are used in children with head and neck pathologies. This allowed us to have an idea of what is being used across institutions and to utilize this information as the basis for the consensus paper.

Ninety-seven institutions responded to at least one survey. The results (supplementary table) show a wide variability in the protocols used in different regions and lack of specific protocols for certain head and neck areas or clinical problems.

Technical notes

- The proposed protocols refer to the minimal required MR sequences recommended to achieve excellent imaging. Optional sequences or specific alternative approaches, depending on the technical conditions (e.g., 1.5 vs 3 T scanners), are also suggested.
- Readers should note that, as a general rule for most of the head and neck pathologies, the need for fat-suppression comes from: (a) T2-hyperintensity of fatty tissue on T2 TSE weighted images (that hides any hyperintense signal from the lesions and/or edema), and (b) T1 hyperintensity of fatty tissue (that hides any contrast enhancement).
- 2D sequences should always be acquired with a minimal slice gap while avoiding slice cross-talk. Such a minimal achievable slice gap is usually 10–20%, depending on the slice selection profile of the applied RF pulses. Zero or negative (overlapping slices) gaps can be achieved by acquiring two separate acquisitions with interleaved slice positions. If not-otherwise specified, a 10–20% slice gap is sufficient for all 2D sequences referred to in this paper.
- We used the technical names of the sequences, but main commercial names (often more familiar to radiologists) are also specified in the abbreviations section and when relevant in the manuscript.
- Multi-shot diffusion weighted images (DWI) or non-EPI DWI are generally better for the skull base and face because these are less sensitive to artifacts. Standard EPI-DWI is, however, acceptable, except for temporal bone imaging in case of suspected cholesteatoma, where non-EPI DWI is the gold standard (see specific section-"temporal bone").
- FS (fat suppression) refers not only to spectral fat saturation techniques, but also to other MR sequences that allow suppression of fat signal. When specific sequences are preferred, for technical or anatomical reasons, this is specified.
- Dixon methods are now widely used and present advantages in comparison to standard FS methods such as: (1) obtaining uniform suppression of fat; (2) providing images with and without fat suppression from a single acquisition, and (3) having the ability to be used with T2 or T1WI, and with spin echo, gradient echo or steady state sequences.

– In addition to the slice thickness, another crucial MR parameter is the in-plane spatial resolution, which is defined by the size of the imaging voxels along the phase and frequency coding axes. It depends on matrix size and the field-of-view (FOV/matrix). For the study of the head and neck region, a high in-plane resolution is required in order to adequately delineate the anatomical structures of this district and lesion extension. For this reason, high acquisition matrices of 448 to 512 should be used, with a field-of-view of 18 to 20 cm, obtaining a 0.4 mm in-plane resolution. As regard to volumetric sequences, an isotropic voxel of 0.6 or 1 mm (depending on the studied region) would be preferable.

Suggested protocols for different head and neck areas and specific pathologies

Orbits

A wide spectrum of pathologies involves the pediatric orbit and peri-orbital soft tissues, including inflammation/infection, tumors, developmental anomalies, and vascular lesions. Furthermore, some abnormalities involving the optic nerves may extend to the optic pathway or other intracranial structures. Therefore, an appropriate approach is required in order to address the range of possible radiological findings [5].

Specific issues when imaging orbits and rationale for optimal MR protocol

The main issues to be addressed when imaging the orbits are: (1) need for high spatial resolution (i.e., thin slices, high resolution matrix) to distinguish and assess the small structures present in this compartment; (2) need to suppress the hyperintense signal of the intra-orbital fat on T1 post-contrast and T2 weighted images; (3) identification of associated intracranial abnormalities, and (4) mitigation of artifacts from surrounding bone and aerated paranasal sinuses.

MRI is the preferred method for characterization of intra-orbital and peri-orbital soft tissue lesions, whereas CT has a complementary role and is chiefly used for assessment of osseous structures. CT should be used as the initial examination for orbital trauma, it is frequently used for the initial assessment of orbital complications of inflammatory/infectious sinus disease and in all instances where it is important to evaluate abnormalities involving bone, for example remodeling/erosion associated with orbital masses and in pre-operative assessment [5]. Detection of ocular calcifications in cases of leukocoria is useful for differential diagnosis, but CT has been largely supplanted by ultrasound (US) and MRI with susceptibility weighted imaging (SWI) [6, 7] since these techniques provide similar and additional information while avoiding the use of ionizing radiation.

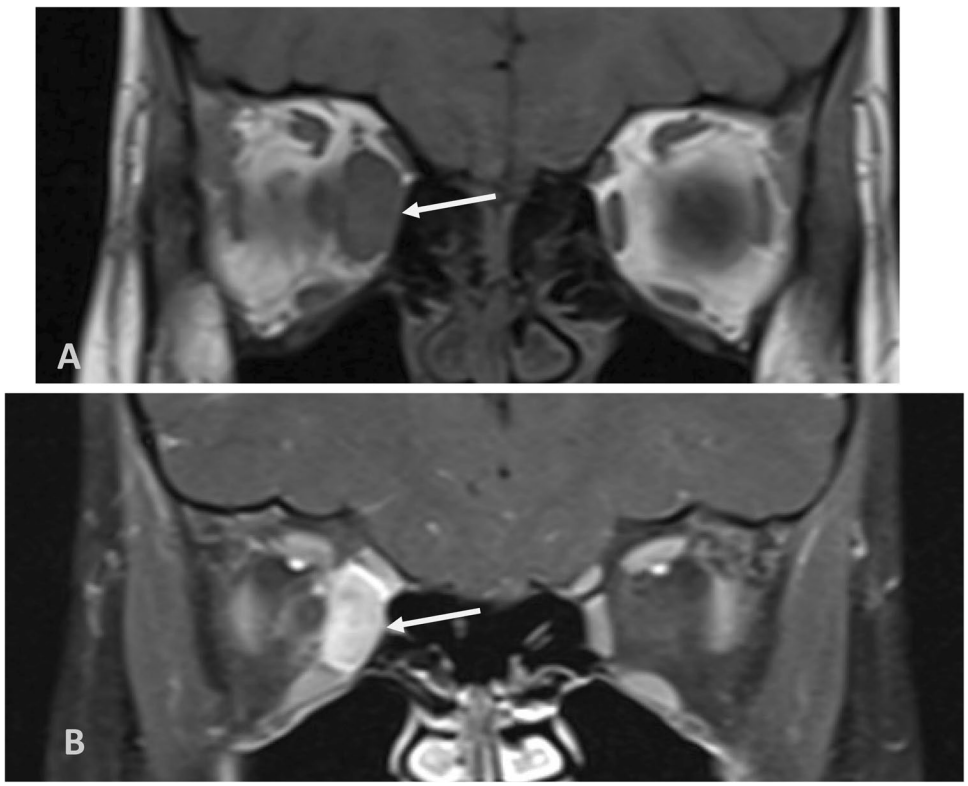

Fig. 1 Nine-year-old female with inflammatory enlargement of the right medial rectus muscle (arrows). Coronal pre-contrast T1WI TSE without fat-suppression **A** shows the enlarged muscle (hypointense) clearly surrounded by hyperintense orbital fat. Conversely, post-contrast T1WI TSE with fat-suppression **B** demonstrates the enhancing muscle well-defined on a background of hypointense (suppressed) fatty signal

Table 1 Proposed orbit protocol

Basic sequences	Plane	Slice thickness (SL)
T2WI TSE with suppression of fat signal	Axial	≤3 mm
T2WI TSE with suppression of fat signal	Coronal	≤3 mm
T1WI TSE	Axial	≤3 mm
T1WI TSE	Coronal	≤3 mm
DWI	Axial	≤3 mm
Post-Gd T1WI TSE with FS	Axial	≤3 mm
Post-Gd T1WI TSE with FS	Coronal	≤3 mm
Optional sequences	**Plane**	**Notes**
MRA TOF or time resolved post-contrast	Axial	In case of suspected vascular malformations
Brain T2WI TSE	Axial	≤4 mm to exclude associated brain pathologies
3D high-resolution heavily T2WI	Axial	≤0.6 mm
Brain Post-Gd 3D T1WI*	Sagittal	1 mm

*In case of suspected intracranial extension of the pathological processes involving the orbits

Of note, SWI has been also suggested as a useful sequence to diagnose retinal hemorrhages in children with suspected non-accidental head injury [8], despite the dilated fundus exams remains the gold standard.

The goal of MR is to help diagnose and delineate the presence of edema, cellulitis and abscesses in cases of orbital and peri-orbital infections [9], to characterize extension and soft tissue characteristics of an orbital mass and to look for intrinsic optic nerve changes. Additionally, high-resolution MR of the extraocular muscles provides useful information regarding the size, shape and position of muscles and delineation of tethering bands, for example in the assessment of strabismus.

Optimally, 3 T MR with a 32- or 64-channel phased-array head coil or appropriate surface coil should be used when available [5], with 3 mm slice-thickness or less. A 1.5 T scanner also provides acceptable image quality when the sequences are optimized [10].

Infection/inflammatory disorders demonstrate hyperintense signal on T2WI and enhancement, but the same is

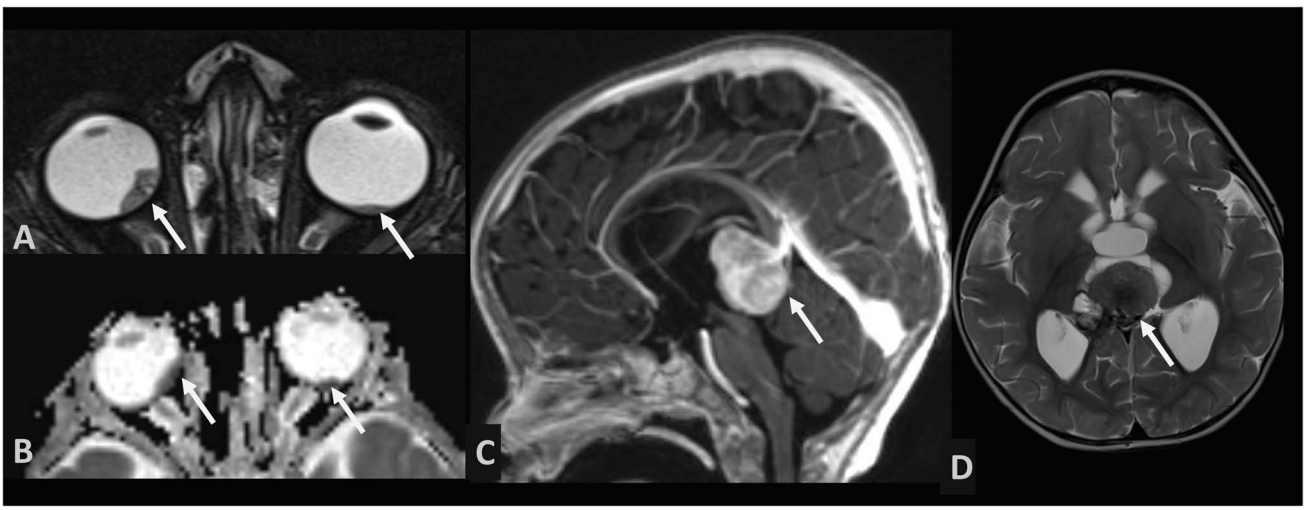

Fig. 2 Fourteen-month-old female with trilateral retinoblastoma (RB). Axial T2WI TSE with fat-suppression **A** and axial DWI ADC **B** show bilateral lesions in the posterior aspect of the globes demonstrating low ADC values (i.e., high cellularity), consistent with RB (arrows). Brain post-contrast sagittal T1WI TSE **C** and axial T2WI TSE **D** sequences demonstrate an associated pineoblastoma (arrows) with triventricular hydrocephalus

true for many intra-orbital masses, thus it is important to acquire T2WI and T1WI TSE post contrast with suppression of fat signal (e.g., T2WI STIR, Dixon fat water separation, or spectral fat saturation). However, fat can be used as a "passive contrast" around a hypointense lesion (neoplastic or inflammatory), thus a pre-contrast T1WI should be acquired without fat suppression (Fig. 1).

DWI is critical for the diagnosis of pus (i.e., abscess) and high cellularity orbital masses (i.e., aggressive tumors) and should always be included. DWI can also help in the assessment of optic nerve ischemia [11]. Ideally, either non-echo planar or multishot EPI DWI sequences, if available, should be acquired in order to mitigate artifacts from surrounding air and bone [12].

SWI is useful to demonstrate blood (for instance in case of traumatic head injury with associated retinal hemorrhage), and calcium (in the differential diagnosis of leukocoria) [5, 7, 13].

MR angiography (MRA) should be added for suspected vascular malformations (such as arteriovenous malformation - AVM - or arteriovenous fistula - AVF -) [14]. If available, a time-resolved post-contrast MRA can be used instead of the non-contrast MRA [15].

Contrast should be used for evaluation of inflammation or neoplasm, unless specific contraindications are present [16].

In case of suspected malignant neoplasm of the orbit, especially parameningeal RMS, T1WI post-contrast of the whole brain is recommended to depict potential intracranial extension, and in such cases, T1WI post-contrast sagittal sequence of the whole spinal axis is also desirable to depict distant leptomeningeal metastases [17].

Finally, it may be useful to add a 3D high resolution heavily T2WI sequence (such as SPACE/CISS/FIESTA-C/VISTA/Cube) to cover cranial nerves III, IV and VI in all patients who present with neuropathies or diplopia.

A proposed orbit protocol is summarized in Table 1.

Retinoblastoma and/or patient with leukocoria

Given the specific imaging characteristics of retinoblastoma (RB) and the requirement for detailed tumor assessment and continued surveillance, RB MR protocols will be discussed separately.

RB is the most common intraocular tumor in children, affecting one or both globes. Bilateral RB (40% of cases) and 15% of unilateral RB are associated with germline mutations of the tumor suppressor gene *RB-1* [18, 19].

Diagnosis is usually obvious at fundoscopy. US is helpful for detection of calcifications (an important diagnostic criterion), as well as tumor-associated complications (retinal

Table 2 Proposed RB protocol

Basic sequences	Plane	Slice thickness
Orbits		
3D high-resolution heavily T2WI*	Axial	≤0.6 mm
T2WI TSE	Axial	≤2 mm
T1WI TSE	Axial	≤2 mm
Post-Gd T1WI FS**	Axial	≤2 mm
Post-Gd T1WI FS**	Sagittal oblique (optic nerve) (affected side only)	≤2 mm
Brain		
T2WI TSE or FLAIR	Axial	≤4 mm
DWI***	Axial	≤4 mm
Post-Gd 3D T1WI	Sagittal	1 mm
Optional sequences	Plane	Notes
3D high-resolution heavily T2WI of the brain (midline)	Sagittal	Suspected pineal embryonal tumor (≤1 mm)
Post-Gd T1WI TSE spinal axis	Sagittal	• extensive optic nerve invasion • suspected intra spinal metastases • trilateral retinoblastoma • slice thickness: ≤3 mm
SWI	Axial	For the assessment of ocular calcifications

*We suggest planning the sagittal oblique sequences using the axial 3D high-resolution heavily T2W [19]

**Or T1WI post contrast without fat suppression and with subtraction. Of note, the use of both T1 WI with and without FS has been suggested for the assessment of invasiveness of retinoblastoma, especially if subtraction images are technically challenging [29]

***Ideally ≤3 mm covering the orbits as well as the brain will demonstrate hypercellularity of the RB as diffusion restricting mass

detachment, hemorrhage etc.). However, MRI is critical for tumor staging and to plan management. RB typically spreads by direct extension into the optic nerve and/or its meningeal sheath into the central nervous system (CNS) or rarely through the bulbar wall into the orbit (delayed presentation) [18, 19]. Furthermore, RB may be associated with midline CNS embryonal tumors (mainly pineoblastoma, less frequently suprasellar tumors), a combination also known as "trilateral" or "quadrilateral" RB. For this reason, a baseline brain MRI is mandatory in RB patients [20–22] (Fig. 2). Although differential diagnosis between benign pineal cyst and cystic pineocytoma may be difficult [23, 24], pineoblastoma is generally solid and large at presentation and can be easily distinguished from a normal pineal gland.

The most frequent clinical findings of retinoblastoma are leukocoria (white pupillary reflex) and strabismus. Several other pathologies, such as persistent fetal vasculature, Coats disease, retinal astrocytic hamartoma and larval endophthalmitis can also cause leukocoria and, therefore, it should be taken into account when considering the differential diagnosis.

Intralesional calcium is the key feature for differentiating retinoblastoma [25] and it is almost always detected by US. MRI with T2* gradient echo or SWI sequence is nearly as accurate as CT for the detection of calcified spots, and without the use of radiation [6, 7].

Additional findings, such as a normal or enlarged globe with RB as opposed to a normal or small globe in many other causes of leukocoria, decreased diffusivity within RB and contrast enhancement patterns are helpful in determining the most appropriate diagnosis or differential diagnosis [26].

Similar to other orbital pathologies, 3T is preferred in these cases [19] and specific sequences with a small field of view should be acquired [27]. Unenhanced axial T1WI without fat suppression and axial post-contrast T1WI (with fat suppression or without fat suppression and subtraction [28]), and sagittal oblique post-contrast T1WI sequences (along the course of the optic nerve) of both eyes are important to demonstrate tumor invasion into the optic nerve and through the layers (choroid and sclera) of the bulbar wall, and in depicting intraocular blood or subretinal fluid with high protein content [19].

Optimized planning of the axial T1WI slices through the posterior part of the optic nerve is key to increasing diagnostic accuracy of optic nerve invasion [19].

At the very least, axial T2WI or FLAIR, post-contrast T1WI (preferably 3D) and axial DWI sequences of the brain should be obtained. A sagittal post-contrast T1WI of the spine is also needed in case of extensive post-laminar optic nerve invasion, evidence of intracranial extension and in patients with trilateral retinoblastoma in order to assess for leptomeningeal tumor dissemination [19].

A proposed RB protocol is summarized in Table 2.

Skull base and skull vault

The skull base refers to the floor of the neurocranium and can be considered as having three components (anterior, central, and posterior). Due to its complex anatomy, presence of fat and muscles, and the presence of multiple foramina transmitting numerous neurovascular structures, an optimized and targeted MR imaging protocol is required [30].

As in other regions, CT has a complementary role in characterizing skull base pathology [31], and it is used primarily to assess bone. However, MRI is the exam of choice for evaluating intracranial extension, assessment of bone marrow lesions, invasion of the cranial nerves and involvement of the adjacent soft tissues [30].

Specific issues when imaging the skull base and vault and rationale for optimal MR protocol

The goals of an effective MR protocol should be to: (1) identify the location and extent of the lesion within and outside the skull; (2) distinguish neoplasm from inflammation/infection, and (3) characterize the lesion.

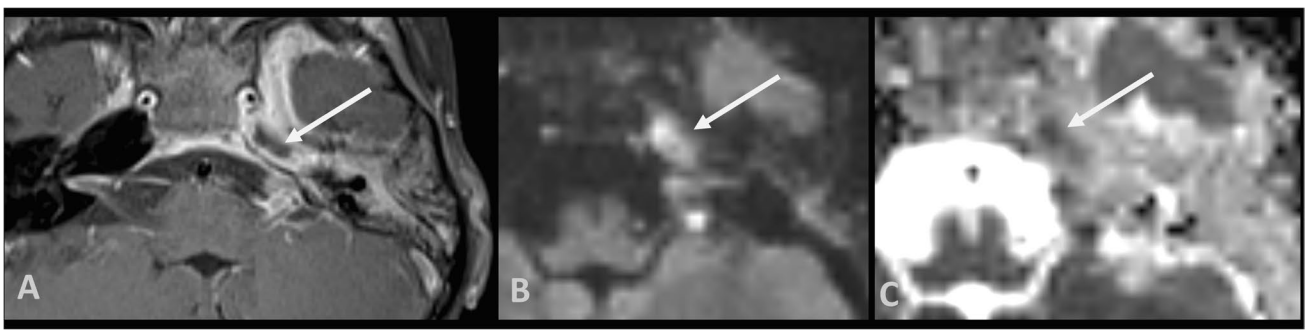

Fig. 3 Six-year-old boy. Axial T1WI TSE with fat-suppression **A**, DWI **B** and ADC maps **C** show a rim-enhancing abscess with restricting core (arrows) in the left apex (evolution of an apicitis)

Table 3 Proposed skull base (+/− vault) protocol

Basic sequences	Plane	Slice thickness
T2WI TSE with FS	Axial	≤3 mm *
T2WI TSE with FS	Coronal	≤3 mm
T1WI TSE	At least two planes or 3D	≤3 mm
DWI	Axial	≤3 mm
Post-Gad T1WI TSE with FS	At least two planes or 3D	≤3 mm or ≤1 mm
Optional sequences	**Plane**	**Notes**
TOF MRA and/or phase contrast/ TOF MRV and/or venography	Axial with MIP 3D reformats	In case of vascular anomalies or venous sinus thrombosis
3D high resolution heavily T2WI	Axial	In case of cranial nerve involvement (e.g.: in parameningeal RMS)
T2WI TSE	Sagittal/Coronal	SL: 2 mm in case of nasal dermoid to look for intracranial extension or in skull base midline encephalocele [39] Coronal T2 is also useful to evaluate the congenital absence or anomalies of the olfactory bulbs in patients with anosmia

*3 mm slice thickness should be used for the skull base. In cases where the skull vault needs to be included in the same examination (for instance in case of metastatic neuroblastoma or other diffuse pathologies), thicker slices (≤5 mm) may be used to reduce imaging time

Fig. 4 Typical LCH lesions demonstrated on axial CT (bone window) with erosion of the frontal bone and soft tissue scalp mass arrows in **A** periorbital lesions with signal on T1WI that is isointense to muscle arrow in **B** and post contrast enhancement arrow in **C**. Marked reduction of vertebral height ("*vertebra plana*") visible on T2WI sagittal of the spine arrow in **D**

Acquired inflammatory skull base pathologies can lead to complications such as osteomyelitis, epidural abscess, subdural empyema, ventriculitis, cerebritis, cerebral abscess, cavernous sinus and venous thrombosis and venous infarction. In these cases, imaging of the whole brain with venous MR angiography and contrast is pivotal [32, 33].

Empyemas and abscesses show restricted diffusion of the purulent core with mural rim-enhancement. DWI and fat-suppressed post contrast sequences are therefore critical for accurate diagnosis of these complications [31] (Fig. 3).

Pre-contrast T1WI without fat suppression is as fundamental as in other head and neck regions because the fat can be used as "passive contrast" around lesions that are often hypointense on T1 [31]. This should be paired with post-contrast fat-suppressed T1WI.

T2WI with fat suppression is important, not only to depict marrow and/or soft tissue edema in inflammatory disorders, but also to demonstrate relatively low signal intensity suggestive of a high nuclear to cytoplasmic ratio in many aggressive tumors. In certain aggressive skull base tumors, such as chordomas and chondrosarcomas, a relatively high signal on T2WI is characteristic and helps in the differential diagnosis more than the pattern of contrast enhancement [34, 35].

Furthermore, thin section, high resolution contrast enhanced MRI with fat suppression plays an essential role in defining tumor extension and perineural tumor spread (PNS), although the latter is more common in adult carcinomas and generally presents as direct extension in children with rhabdomyosarcomas (RMS) [36].

Table 4 Proposed LCH protocol

Sequences	Plane	Slice thickness
Brain and skull (including the vertex and the skull base)		
T1WI 3D*	3D with MPR reformats	1 mm
FLAIR	Coronal	≤4 mm
T2WI TSE	Axial	≤4 mm
DWI	Axial	≤4 mm
Post-Gad T1WI TSE with FS	at least two planes or 3D	≤4 mm or 1 mm (if 3D)
Sellar region (optional)		
T1WI TSE post contrast**	Sagittal midline	≤2 mm
3D high resolution heavily T2WI ***	Sagittal midline	≤0.6 mm
Spine (at diagnosis and follow-up if lesion present or clinically suspected)		
T2WI STIR [45]	Sagittal	≤3 mm
T1WI TSE [45]	Sagittal	≤3 mm

* This sequence allows high resolution images of the brain but also skull and pituitary region for the visualization of the posterior pituitary "T1 bright spot". Alternatively, use of T1WI sagittal (pre- and post- contrast) instead of 3D T1WI of the sellar region is also acceptable

** Can be added in case of suspected enhancing sellar mass on brain images

*** Some authors suggest this as the best sequence for the evaluation of the stalk, but in most of the cases, 3D T1WI of the brain or T1WI thin slices of the sella are sufficient [46, 47]

Time of flight (TOF) MR angiography (MRA) and dynamic MRA may be helpful in case of vascular anomalies, while MR venogram should be added when venous thrombosis is suspected [37].

The same imaging principle applies to the skull vault, which is particularly significant in children because of typical skull localizations of Langerhans cells histiocytosis (LCH) and neuroblastoma metastasis [38].

A proposed skull base (+/− vault) protocol is summarized in Table 3.

The coverage should be till the inferior margin of C2.

LCH

Langerhans Cell Histiocytosis (LCH) presents with typical involvement of the skull base (including temporal bone) and vault. However, given the involvement of other regions of the body, particularly intracranially and in the spine, a more specific imaging approach is needed in cases of confirmed or suspected LCH [40].

LCH typically presents with bone lesions, and the most common locations are the skull and long bones [41]. Skull lesions on X-Ray and CT have a typical lytic, "punched-out" appearance with characteristic beveled edges due to asymmetric erosion of the inner and outer cortices (Fig. 4A) and with no internal osseous/chondral matrix or periosteal reaction. Typically, these lesions appear hyperintense on T2WI, isointense to muscle on T1WI, and enhance after contrast administration [40] (Fig. 4B and C). However, atypical appearances do occur, such as intralesional hemorrhage [42]. The characteristic appearance of these lesions in CT and plain radiographs provides diagnostic and complementary information to MRI, at least at first presentation. Nevertheless, MRI is critical for complete staging of the disease.

Vertebra plana (i.e., reduction of the vertebral body height) is the most common imaging finding in the spine, and MR images reveal variable signal on T1WI and hyperintense signal on T2WI together with reduction of the vertebral height (Fig. 4D).

CNS involvement is less common, and is primarily characterized by hypothalamic infiltration causing diabetes insipidus. The most typical MR finding is loss of the normal posterior pituitary bright spot on non-enhanced T1WI, with associated infundibular thickening, which is best appreciated on contrast enhanced MR sequences [40]. For these reasons, specific sequences for assessment of the pituitary region are needed. Temporal bone involvement is very often bilateral with sparing of the otic capsule and with mild clinical features in spite of the aggressive appearance on MRI.

Patients may also present with brain lesions, in particular cerebellar and in the basal ganglia, which appear to be related to auto-immune demyelination and they are the second most common intracranial LCH manifestation [43, 44].

A proposed LCH protocol is summarized in Table 4.

Suprahyoid and infrahyoid neck

Neck masses are frequent in children and may have numerous etiologies (congenital, acquired, inflammatory, neoplastic or vascular).

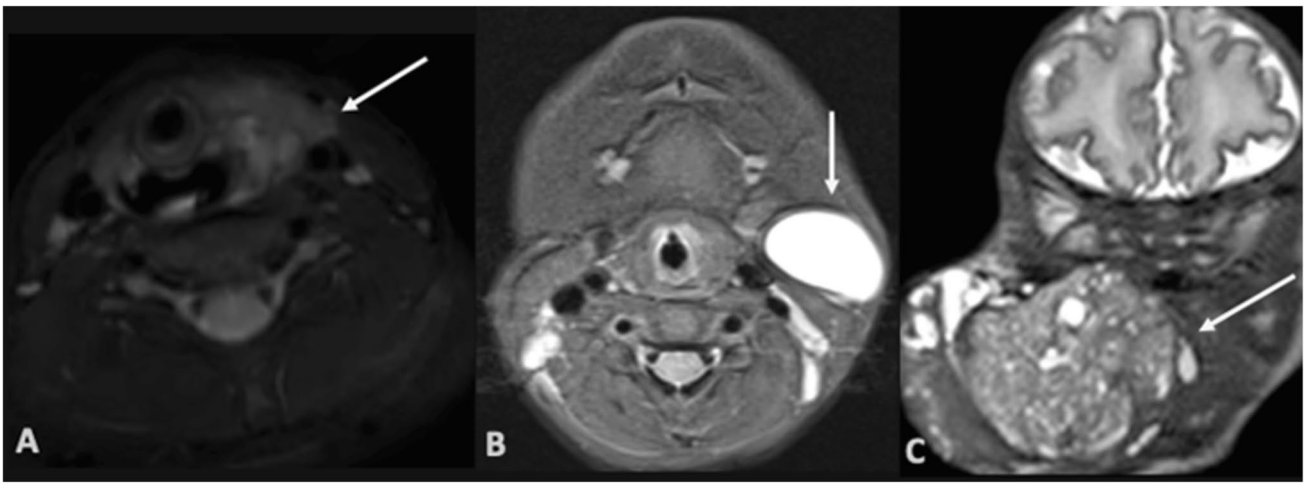

Fig. 5 T2WI STIR in 3 patients with infrahyoid pathology. **A** toddler with left neck infection (arrow) probably secondary to infected 4th branchial cleft anomaly (note the ill-defined edema). **B** young female with left 2nd branchial cleft anomaly (arrow, note the sharp margin of the homogeneous cystic lesion). **C** large teratoma extending in the supra and infrahyoid compartments in a neonate with solid-cystic complex structure (arrow)

For these reasons, the neck requires a specific and appropriate multimodality imaging approach, including radiographs, US, CT and MR [48].

US is often the initial imaging exam in superficial masses, helps distinguish cystic versus solid lesions, and it is useful for detecting mineralization (as in phleboliths) [49, 50].

Specific issues when imaging the suprahyoid and infrahyoid neck and rationale for optimal MR protocol

Recent innovations in MRI scans and sequence advances have increased the advantages in using MRI over CT [51]. MR protocols for studies of this region should always include sequences with a slice thickness of ≤ 3 mm (unless the lesion being examined is large), in order to better depict anatomical structures and avoid "partial volume effect" artifacts. However, obtaining thin sections, high resolution slices, results in decreased signal-to-noise ratio and an increased time of acquisition which may cause artifacts related to movement: namely breathing, swallowing and vessel pulsation artifacts. These issues can be solved by managing sequence parameters (e.g., repetition and echo times, acquisition and reconstruction matrices, field of view, number of signal averages/acquisitions, bandwidth, etc.) or by the use of techniques for accelerating MRI data acquisition (e.g., parallel imaging, compressed sensing). Radial k-space sampling sequences can also be adopted, which are typically less sensitive to motion [4].

Table 5 Proposed neck protocol

Basic sequences	Plane	Slice
T1WI TSE	Axial	≤ 3 mm
T2WI TSE with FS	Axial	≤ 3 mm
T2 TSE with FS	Coronal	≤ 3 mm
T2WI TSE (optional)	Axial	≤ 3 mm
DWI	Axial	≤ 3 mm
Post-Gd T1WI TSE with FS*	Axial	≤ 3 mm
Post-Gd T1WI TSE with FS *	Coronal	≤ 3 mm

*Volumetric gradient-echo sequences with fat suppression (e.g., VIBE, THRIVE, LAVA) may also be used after contrast administration

Surface coils, applied to the patient's neck, are advantageous for the study of superficial regions and provide higher signal–noise ratio, allowing for superior spatial resolution. For this reason, surface coils are particularly useful in the study of the larynx, cervical trachea and isolated superficial lesions in which image acquisition can be focused without the need for a large field of view. When using phased-array surface coils, parallel-imaging techniques can similarly be used to reduce the acquisition time [52].

Anatomical MR sequences are helpful in defining anatomical relationships of the lesion and in providing soft tissue characterization to differentiate between solid, cystic mixed, fatty or vascular nature (Fig. 5) [4].

In addition, DWI helps in characterizing hypercellular (e.g., aggressive tumors), suppurative and benign lesions [32] [4].

Special considerations for imaging of the neck include presence of dental braces, palate expanders, metallic implants, as well as dealing with failure of spectral fat-suppression related to lesions in the region of the chin and base of neck. T2WI STIR images are preferred over spectral

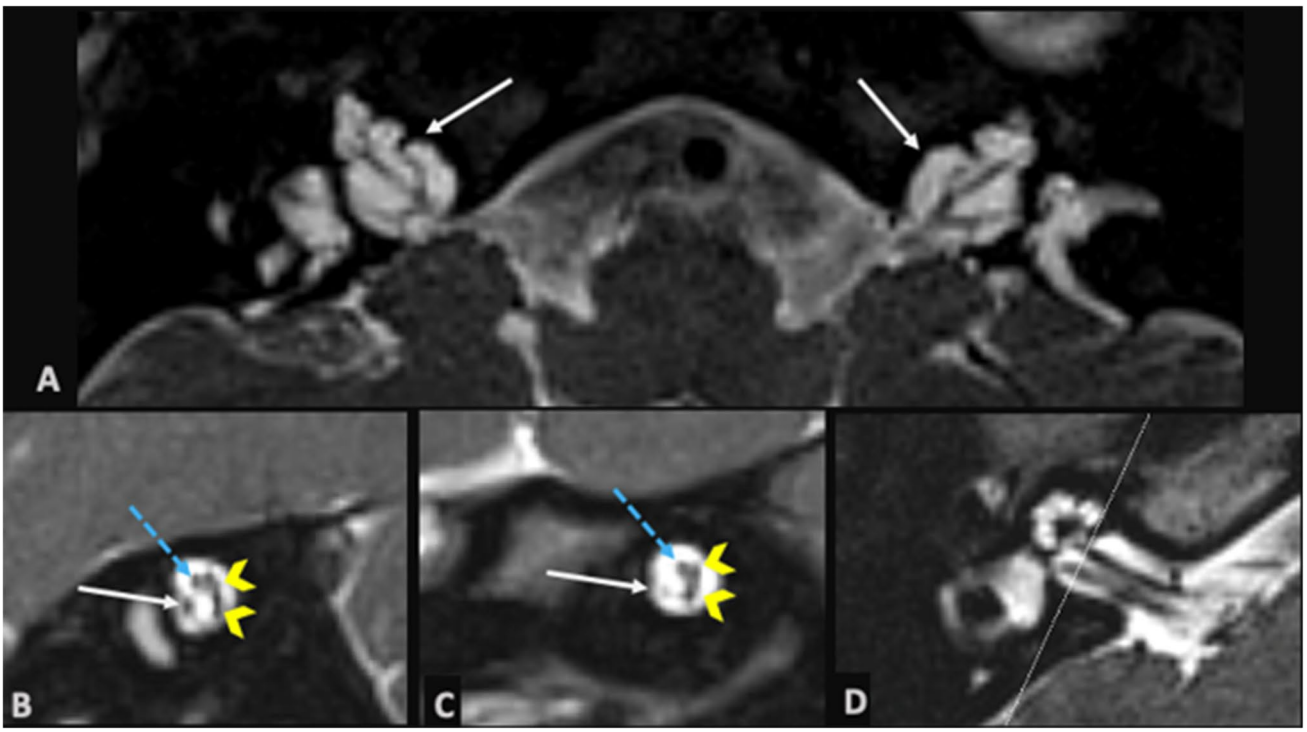

Fig. 6 Axial 3D T2WI in a male patient with X-linked deafness with mixed hearing loss and stapes gusher, showing bilateral incomplete partition type 3 cochlear malformation arrows in **A** with enlarged IACs and absent modioli. Parasagittal right and left **B** and **C** 3D T2WI in another patient with unilateral hearing loss, showing the presence of VII cranial nerve (blue dashed arrow) vestibular nerves (yellow arrowheads) and cochlear nerve (white arrow). Note that the cochlear nerve is hypoplastic on the left, explaining the hearing loss. **D** shows the acquisition plane on axial 3D T2WI also demonstrating normal cochlear anatomy

fat-suppressed T2WI and T1WI with 2- or 3-point Dixon fat–water separation is preferred over spectral fat-suppressed T1WI in such situations [53].

A proposed neck protocol is summarized in Table 5.

Additional sagittal sequences before and after contrast administration are recommended in case of lesions involving the epiglottis or the retropharyngeal/prevertebral spaces.

Temporal bone

Specific issues when imaging the temporal bone and rationale for optimal MR protocol

The main indication for temporal bone imaging in children is hearing loss.

Hearing loss can be divided into three forms:

- *sensorineural hearing loss* (SNHL) refers to a problem occurring in the inner ear or the neural pathway to the auditory cortex;
- *conductive hearing loss* (CHL) occurs when the conduction of the sound from the outer to the inner ear is impaired (e.g., ossicular abnormalities or inflammation of the tympanic cavity);
- *mixed hearing loss* is a combination of the two.

Diagnostic imaging is fundamental to detect the etiology of hearing loss and to establish the appropriate treatment (for instance, suitability for cochlear implant).

CT is utilized to depict the bone of the external auditory canal, the ossicles, the walls of the middle ear, the otic capsule and the facial nerve canal [54–56] and it is the exam of choice for the evaluation of CHL. Multidetector CT is the most widely used CT for the temporal bone images, however cone beam CT (CBCT) is considered the gold standard, particularly for conductive hearing loss, it offers the advantage of a higher resolution and a lower radiation dose, compared to MDCT but is more sensitive to motion artifacts which may be relevant in children.

MRI provides detail of the fluid-containing structures of the inner ear and allows direct visualization of the vestibulocochlear and facial nerves [57, 58]. Thus, it is used, sometimes with CT corroboration, for the evaluation of SNHL and to confirm the presence of the cochlear nerve prior to cochlear implantation [59] (Fig. 6).

A limited fast brain MR should also be obtained for the evaluation of SNHL in order to detect brain parenchymal changes (e.g., polymicrogyria in case of prenatal infections

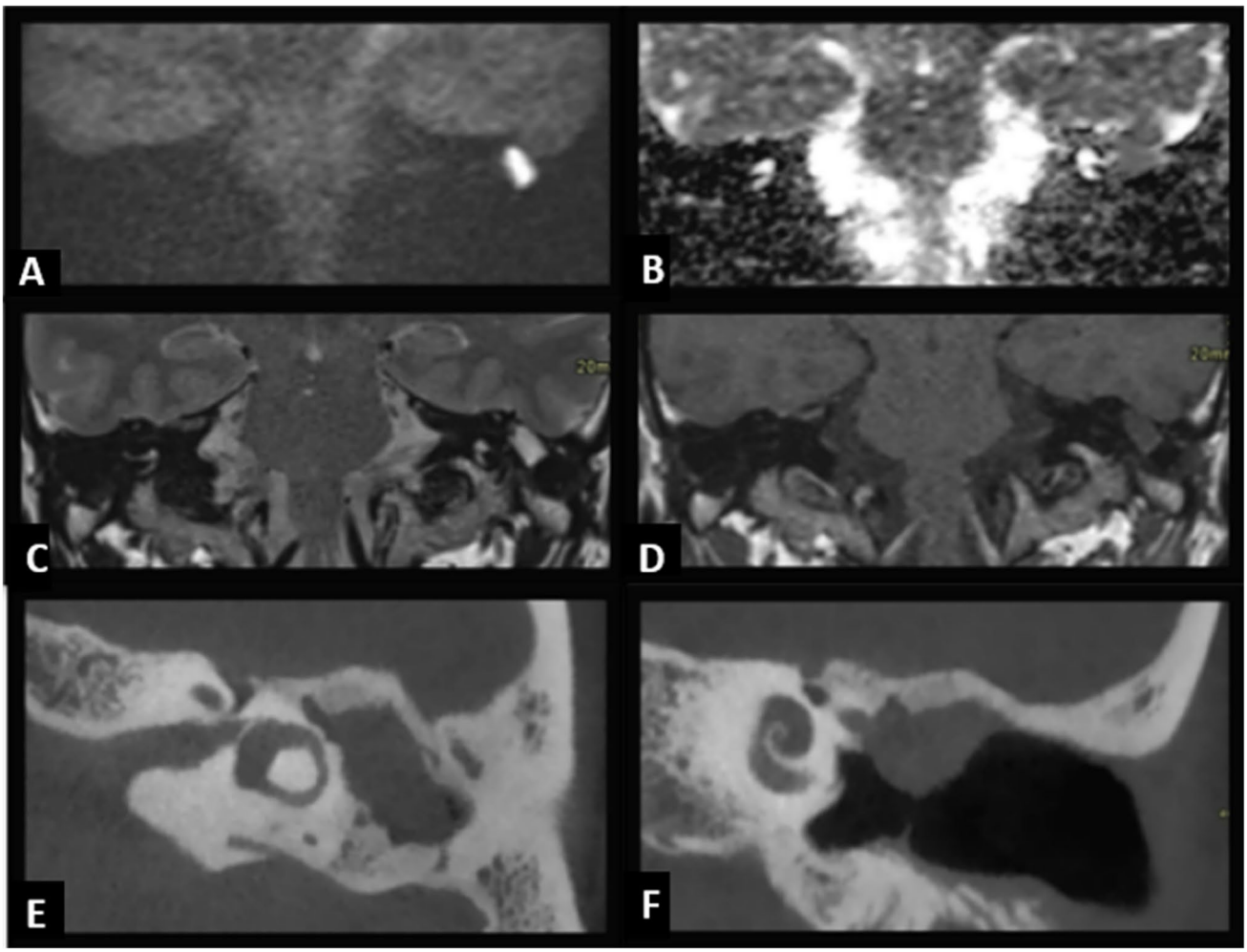

Fig. 7 Patient with prior canal wall up tympanoplasty for cholesteatoma, presenting now with clinical suspicion at otoscopy of a recurrent cholesteatoma. Coronal non-EPI DWI with $b = 1000$ s/mm^2 **A**, ADC map **B**, T2-weighted image and T1-weighted image through the middle ear, slice thickness of 2 mm **C** and **D**. The lesion shows a high intensity on non-EPI DWI with a clear signal drop on ADC map. It displays an intermediate intensity on T2WI and shows a low signal intensity on T1WI. These signal intensities are compatible with cholesteatoma. Axial and coronal reformations of a CBCT **E** and **F**—performed prior to surgery—confirms the presence of a recurrent cholesteatoma at the upper border of the tympanic membrane. MRI diagnosis of a cholesteatoma relies on non-EPI DWI, T2 and T1-weighted images, as illustrated above

Table 6 Proposed temporal bone and cholesteatoma protocol

Basic sequences	Plane	Slice
Non-EPI DWI or multi-shot EPI *	Coronal	≤ 3 mm
Non-EPI DWI or multi-shot EPI *	Axial (optional)	≤ 3 mm
T2WI TSE**	Coronal	≤ 3 mm
T2WI TSE**	Axial	≤ 3 mm
T1WI TSE	Axial or Coronal	≤ 3 mm

*Non-EPI DWI generally preferred when available

**or a 3D T2WI with coronal and axial reformats, which is preferred by some for the higher spatial resolution

associated with deafness such as cytomegalovirus, lesions involving the auditory pathway, or neurogenetic disorders associated with deafness such as mitochondrial disorders) [55, 60].

The MR sequences used for the inner ear are 3D high resolution heavily T2WI with ≤ 0.6 mm voxel size, preferably on a 3 T system. Such sequences facilitate identification of inner ear malformations as well as loss of normal fluid signal suggestive of labyrinthine fibrosis or ossification [55, 61].

Cranial nerves VII and VIII can be seen in the internal auditory canals (IACs) traversing the cerebellopontine angle cisterns on parasagittal reformats of the volumetric heavily T2WI sequence [62, 63]. However, direct sagittal oblique 3D T2WI are very helpful to accurately assess the precise size of the cochlear nerves especially in narrowed/dysmorphic IACs (Fig. 6B, C and D).

Unlike the protocol in adults, post-contrast fat-suppressed high resolution T1WI is not required for the assessment of congenital hearing loss. Contrast is reserved for patients suspected of having acquired SNHL due to inflammatory (auto-immune), infectious (labyrinthitis), or neoplastic etiologies [64].

Finally, for the clinical suspicion of cholesteatoma, particularly recurrent cholesteatoma, a non-EPI (ideally coronal) or a multi-shot EPI diffusion weighted sequence should be acquired, since cholesteatoma typically shows marked diffusion restriction in comparison to inflammatory diseases involving the same location [61, 65–67] (Fig. 7).

In our personal experience and according to recent literature, non-EPI DWI is the gold standard and preferable to a multi-shot EPI DWI [68, 69]; nevertheless, the latter is still acceptable in case an optimized non-EPI DWI isn't available [66, 70, 71]. However, standard EPI DWI should be always avoided in these cases.

Correlation to ADC map is required as well as to T2WI sequences to localize the lesion. Gadolinium administration is no longer required for cholesteatoma imaging except if a complication, such as meningitis and ear infection, is suspected [72, 73]. In case of primary or recurrent cholesteatoma, high resolution T1WI should also be performed to differentiate it from blood or high protein content. CT is only required in a pre-operative setting as an anatomical roadmap and in order to evaluate the ossicular chain [73].

A proposed temporal bone and cholesteatoma protocol is summarized in Table 6.

Pre-operative MR in cochlear implant patients

Cochlear implant centres have a variable approach to pre-operative implant imaging, and both MRI and CT have potential advantages. These exams help evaluate anatomic variants and anomalies that pose surgical hazards (e.g., CT is useful for diagnosis of oval window atresia with aberrancy of the tympanic facial nerve canal) and to confirm the presence/morphology of the cochlea and cochlear nerve (the latter only visualized on MRI) [74]. In the pediatric population, hearing loss is often associated with complex syndromes, so the combination of high resolution CT and MR of the temporal bone with general imaging of the brain with MRI minimizes the chance of missing important radiological findings [75].

CT allows the evaluation of mastoid pneumatization, provides detail of other osseous structures (bony labyrinth, ossicular chain, etc.) and allows for excellent visualization of the facial nerve canal.

Of note, while current literature suggests the use of both CT and MRI in pre-operative planning, there is a recent direction toward limiting CT to specific cases with the use of black bone MRI as a possible MR alternative to CT, but this technique still has limitations and more studies are necessary to assess its reliability [76].

Although not ideal, especially in patients with complex ear malformations, a fast protocol has also been proposed and may reduce the needs of sedation [77].

A proposed hearing loss and pre-cochlear implant protocol is summarized in Table 7.

MR may also be required in patients with cochlear implants (CI) to evaluate postoperative complications (e.g., meningitis) or other conditions associated (e.g., neurofibromatosis type 2, CHARGE syndrome, brain tumors) [78].

Numerous issues are encountered performing MRI in patients with CIs, so various guidelines have been proposed to limit artifacts, demagnetisation and the rotational force of the MRI scan that poses the risk of implant magnet migration causing pain and damage to the surrounding soft tissues.

Table 7 Proposed hearing loss and pre-cochlear implant protocol

Sequence	Plane	Slice thickness
Brain		
T2WI TSE *	Axial	≤ 4 mm
FLAIR (optional)	Coronal or 3D	≤ 4 mm/≤ 1 mm
3D T1WI ** (optional)	Sagittal + reformats	1 mm
Temporal bone (3T scanner preferred)		
3D high resolution heavily T2WI	Axial with coronal reformats	≤ 0.6 mm
3D high resolution heavily*** T2WI	Right parasagittal	≤ 0.6 mm
3D high resolution heavily T2WI ***	Left parasagittal	≤ 0.6 mm

* Replaced by dual-echo, axial STIR (or FSE or TSE T2 sequences with increased TR and TE) in patients under 2 years of age to account for the increased water content in the unmyelinated brain [74]

** Increases the sensitivity in diagnosing areas of polymicrogyria in children with deafness due to pre-natal infections

*** Parasagittal 3D T2WI are particularly critical on 1.5 T scanner or in case of narrowed/dysplastic internal auditory canals; an optimized axial 3D T2WI sequence on a 3 T scanner should provide enough signal-to-noise for parasagittal reformats of the native axial

Depending on the implant model, MRI can be undertaken at 1.5 T or 3 T (the magnet of the CI must be removed in this last case): it must be emphasized that the risk of painful magnet dislocation, magnet demagnetization and imaging artifacts are reduced by decreasing the strength of the magnetic field. Artifacts can also be limited by performing higher readout bandwidth, lower TE, or view angle tilting sequences or specific imaging techniques such as MAVRIC-SL (multi acquisition with variable resonance image combination—selective) or SEMAC (Slice Encoding for Metal Artifact Correction) [79, 80]. Recently, freely rotating magnets that align with the MR magnetic field have been developed; this eliminates the risk of soft tissue damage due to rotational forces [78].

Paranasal sinuses and nasopharynx

Specific issues when imaging sinuses and nasopharynx and rationale for optimal MR protocol

A large variety of pathologies may involve the paranasal sinuses/nasopharynx, including inflammation, post-traumatic lesions and soft-tissue masses. Rhinosinusitis is extremely common, unlike sinonasal neoplasms, which are rare and constitute 3% of head and neck tumors [81]. The more commonly encountered pediatric sinus tumors vary with age. Malignant tumors include metastatic disease (e.g., neuroblastoma, leukemia), and primary malignancies such as rhabdomyosarcoma and lymphoma. Unlike adults, squamous or undifferentiated carcinoma is exceptionally uncommon. The imaging approach in children is similar to adults and the MR protocols are similar for sinuses, pharynx and oral cavity.

CT is used in children less often than in adults. In fact, CT is usually the first imaging modality to evaluate bone, and it is superior to MRI in characterization of fibro-osseous lesions [82, 83], it helps assess anatomical variants, and it is used for pre-operative planning. However, chronic rhinosinusitis and endoscopic sinus surgery are much more common in adults and anatomical variants are less concerning in children, where the full development of the paranasal sinuses occurs after 12–14 years of age. Furthermore, acute rhinosinusitis generally does not require imaging unless intracranial/orbital complications are present, in which cases MRI is better.

The CT protocols and evaluation of this anatomical region are outside the scope of this paper, but we suggest applying a rigorous structured approach when reporting paranasal sinuses CT scans as suggested by O'Brien and colleagues [84].

MRI, instead, is a useful modality to characterize inflammation/infection, sinonasal masses and to depict the extent of disease. Thin section high resolution sequences [85] in at least 2 planes are required, in particular sagittal sequences are indicated mainly when anterior skull base lesions are suspected [82].

T2WI FS helps in differentiating benign from malignant lesions. Benign lesions such as polyps are hyperintense on T2WI with a peripheral enhancement on post-gadolinium T1WI, whereas aggressive neoplastic lesions often show intermediate signal intensity on T2WI due to their higher cellularity [82] and decreased diffusivity. T2WI may also help in differentiating neoplastic lesions from chronic fungal lesions which appear hypointense on T2WI [86]. Sometimes high density proteinaceous secretions can show T2WI hypointensity and T1WI hyperintensity [87] reflecting protein concentration.

Post-contrast sequences in cases of aggressive pediatric tumors such as RMS, show heterogeneous enhancement and highlight the presence of necrosis. Hemorrhagic lesions (bright areas on T1WI) may also be found [88] in a wide spectrum of diseases.

Contrast enhanced T1WI FS is also useful to evaluate epidural, dural and subdural involvement in infections or neoplasms [89].

DWI may help in differentiating neoplastic from inflammation and post-treatment inflammatory changes from recurrences [90]; furthermore, as in other compartments, it may diagnose pus in pyogenic abscesses.

Additional sequences include DCE perfusion MR imaging for inflammation/tumor differentiation [91, 85].

A proposed paranasal sinuses protocol is summarized in Table 8.

Table 8 Proposed paranasal sinuses protocol

Basic sequences*	Plane	Slice thickness
T2WI TSE FS	Coronal and axial	≤ 3 mm
T1WI TSE WI	Coronal	≤ 3 mm
DWI	Axial	≤ 4 mm
Post-Gad T1WI TSE FS	Ideally 3D with reformats	≤ 1 mm or ≤ 3 mm

*Some authors prefer adding a standard T2WI and post-Gad T1WI without FS to the protocol to better delineate the anatomical boundaries of the disease. Sagittal T2WI can be also added if specifically needed

Advanced techniques

Several advanced MRI techniques have been developed with promising applications in the pediatric head and neck. Particularly in children, there is an inherent tradeoff between scan time and information. Depending on the suspected disease process, advanced techniques can be selectively applied to elevate overall diagnostic performance by providing enhanced and complementary information about tissue properties [92, 93]. These techniques are not yet standardized

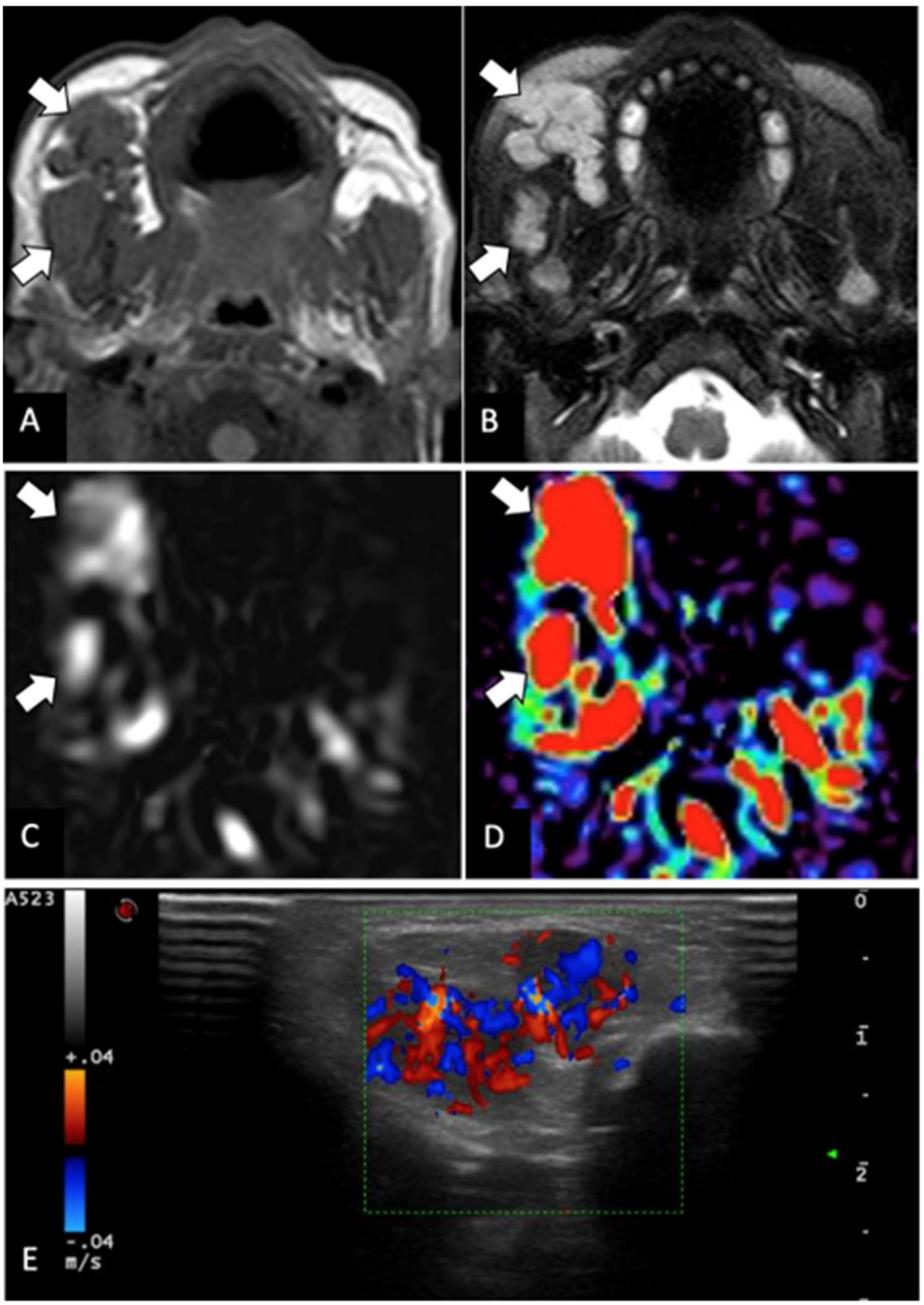

Fig. 8 Brain MRI and US in a preterm neonate studied at term-equivalent age for germinal matrix hemorrhage showing as an incidental finding a facial soft-tissue hemangioma. **A** Axial T1-weighted and **B** T2-weighted images reveal multiple T1-isointense and T2-hyperintense lesions in the right cheek (thick arrows), extending posteriorly toward the parotid space. **C** Gray scale and **D** Colored Pulsed ASL (pASL) perfusion maps demonstrate high signal of the lesions in keeping with the diagnosis of infantile hemangioma (thick arrows). **E** Ultrasound with color doppler confirms the presence of high flow signals within the lesions

for the use in head and neck images, so we will just briefly summarize their potential, future applications.

Enhanced tissue characterization

Zero and ultrashort echo-time techniques enable visualization of short-T2 tissues (e.g., cortical bone), offering a potential alternative to CT without the use of ionizing radiation [94, 95].

Magnetic resonance elastography (MRE) utilizes an external driver to transmit transverse shear waves through tissue and compute stiffness metrics. MRE is already clinically utilized in the pediatric liver to measure stiffness in various pathologic conditions. Emerging applications in the pediatric head include preoperative calculation of pituitary/brain tumor consistency and assessment of tumor-normal tissue interfaces for surgical planning [96]. Possible applications in the neck soft

tissue characterization (e.g., nodes) are being developed [97].

Ultra-high-field imaging (≥ 7 Tesla) offers exquisite signal-to noise-ratio, spatial and contrast resolution, which shows potential for evaluating microanatomy and small subtle lesions of the orbits, pituitary, and skull base. The benefits of 7 Tesla must be balanced against imaging times, artifacts, and patient access and safety issues [98]. The use of 7 Tesla imaging for the head and neck is particularly promising for evaluation of the inner ear structures [99].

Anatomic modeling and visualization have numerous applications in promoting patient and family understanding, medical trainee education/simulation, and surgical preoperative planning and intraoperative navigation. Interactive virtual, augmented, and mixed reality programs are increasingly being adopted by interventional radiologists and surgeons worldwide [100, 101].

Perfusion and flow imaging

Perfusion imaging can be performed with non-contrast (arterial spin labeling — ASL) and contrast (dynamic susceptibility contrast, dynamic contrast enhanced) techniques. ASL imaging of cutaneous vascular anomalies in children, has been reported as showing specific signal intensity patterns thus providing additional value when compared to conventional MR sequences, particularly with high flow vascular lesions and vascular tumors (Fig. 8) [102].

Vessel wall imaging with luminal signal suppression can be performed both intracranially and extracranially to evaluate in suspected vasculopathies affecting large, medium, and/or small vessels [103].

Metabolic imaging

Spectroscopic evaluation of chemical composition in the head and neck is currently challenging due to the long imaging times, complex structures requiring coil optimization and shimming, and abundant water and fat signals that must be suppressed. Most applications have focused on proton MRS and standard ^{1}H metabolite concentrations for differentiating benign from malignant conditions; other nuclei are challenging to detect via MRS at normal clinical field strengths [104].

Chemical exchange saturation transfer (CEST) imaging is an alternative MRI approach that can be used to assess metabolic processes through continuous radiofrequency saturation and exchange of signal between free water and solutes (endogenous diamagnetic or exogenous paramagnetic substances). The most promising applications are in distinguishing benign from malignant conditions and recurrent tumor from treatment effects [105].

Positron emission tomography (PET)-MRI can be performed sequentially with image co-registration, or using a special hybrid unit for simultaneous image acquisition. PET/MRI provides concurrent anatomic and metabolic information, which may be helpful for the analysis of the head and neck regions in particular with the use of whole body scans [106, 107].

Conclusions

MR imaging in pediatric head and neck pathology is very complex, it depends on the region of interest and poses several challenges. We propose standardized MR protocols to help the readers in approaching pediatric head and neck pathologies and to help minimize the variability and maximize diagnostic efficiency. We discussed the added value of CT in specific areas or diseases, basics and optional/alternative MR sequences depending on the clinical problem/region of interest. This consensus paper has been endorsed by many international scientific societies. The members of the COMPS group recognize that this is intended as a work-in-progress, and further improvement and updates of the present consensus statement will be necessary overtime.

Supplementary Information The online version contains supplementary material available at https://doi.org/10.1007/s00234-022-02950-9.

COMPS contributors:

Alessandro Bozzao, Jan Sedlacik, Camilla Rossi Espagnet, Daniela Longo, Alessia Carboni, Lorenzo Ugga, Stefania Picariello, Giacomo Talenti, Sniya V. Sudahakar, Martina Di Stasi, Ulrike Löbel, Robert Nash, Kaukab Rajput, Olivia Carney, Davide Farina, Richard Hewitt, Olga Slater, Jessica Cooper, Gennaro D'Anna, Gul Moonis, Andrea Rossi, Domenico Tortora, Cesar Augusto Alves, Asif Mazumder, Faraan Khan, Teresa Nunes, Owen Arthurs, Hisham Dahmoush, Renato Cuocolo, Pablo Caro-Dominguez, Arastoo Vossough, William T. O'Brien, Asthik Biswas, Catriona Duncan, Lennyn Alban.

Funding This work was supported by the National Institute for Health Research, GreatOrmond Street Hospital Biomedical Research Centre. No funding was received for this study.

Declarations

Conflict of interest The authors have no relevant financial or non-financial interests to disclose.

Ethical approval Approval was not necessary for this kind of manuscript.

Informed consent Consent was not necessary for this kind of manuscript.

References

1. Avula S, Peet A, Morana G et al (2021) European Society for Paediatric Oncology (SIOPE) MRI guidelines for

imaging patients with central nervous system tumours. Childs Nerv Syst 37:2497–2508. https://doi.org/10.1007/s00381-021-05199-4
2. Saunders DE, Thompson C, Gunny R et al (2007) Magnetic resonance imaging protocols for paediatric neuroradiology. Pediatr Radiol 37:789–797. https://doi.org/10.1007/s00247-007-0462-9
3. Vargas M-I, Becker M, Garibotto V et al (2013) Approaches for the optimization of MR protocols in clinical hybrid PET/MRI studies. MAGMA 26:57–69. https://doi.org/10.1007/s10334-012-0340-9
4. Widmann G, Henninger B, Kremser C, Jaschke W (2017) MRI sequences in head & neck radiology - state of the art. Rofo 189:413–422. https://doi.org/10.1055/s-0043-103280
5. Vachha BA, Robson CD (2015) Imaging of pediatric orbital diseases. Neuroimaging Clin N Am 25:477–501. https://doi.org/10.1016/j.nic.2015.05.009
6. Galluzzi P, Hadjistilianou T, Cerase A et al (2009) Is CT still useful in the study protocol of retinoblastoma? AJNR Am J Neuroradiol 30:1760–1765. https://doi.org/10.3174/ajnr.A1716
7. Rodjan F, de Graaf P, van der Valk P et al (2015) Detection of calcifications in retinoblastoma using gradient-echo MR imaging sequences: comparative study between in vivo MR imaging and ex vivo high-resolution CT. AJNR Am J Neuroradiol 36:355–360. https://doi.org/10.3174/ajnr.A4163
8. Bhatia A, Mirsky DM, Mankad K et al (2021) Neuroimaging of retinal hemorrhage utilizing adjunct orbital susceptibility-weighted imaging. Pediatr Radiol 51:991–996. https://doi.org/10.1007/s00247-020-04897-6
9. Wells RG, Sty JR, Gonnering RS (1989) Imaging of the pediatric eye and orbit. Radiographics 9:1023–1044. https://doi.org/10.1148/radiographics.9.6.2685932
10. Nagesh CP, Rao R, Hiremath SB, Honavar SG (2021) Magnetic resonance imaging of the orbit, Part 1: basic principles and radiological approach. Indian J Ophthalmol 69:2574–2584. https://doi.org/10.4103/ijo.IJO_3141_20
11. Chen JS, Mukherjee P, Dillon WP, Wintermark M (2006) Restricted diffusion in bilateral optic nerves and retinas as an indicator of venous ischemia caused by cavernous sinus thrombophlebitis. AJNR Am J Neuroradiol 27:1815–1816
12. Feeney C, Lingam RK, Lee V et al (2020) Non-EPI-DWI for detection, disease monitoring, and clinical decision-making in thyroid eye disease. AJNR Am J Neuroradiol 41:1466–1472. https://doi.org/10.3174/ajnr.A6664
13. Zuccoli G, Panigrahy A, Haldipur A et al (2013) Susceptibility weighted imaging depicts retinal hemorrhages in abusive head trauma. Neuroradiology 55:889–893. https://doi.org/10.1007/s00234-013-1180-7
14. Steinklein JM, Shatzkes DR (2018) Imaging of vascular lesions of the head and neck. Otolaryngol Clin North Am 51:55–76. https://doi.org/10.1016/j.otc.2017.09.007
15. Krishnamurthy R, Muthupillai R, Chung T (2009) Pediatric body MR angiography. Magn Reson Imaging Clin N Am 17:133–144. https://doi.org/10.1016/j.mric.2008.12.004
16. Sepahdari AR, Aakalu VK, Kapur R et al (2009) MRI of orbital cellulitis and orbital abscess: the role of diffusion-weighted imaging. AJR Am J Roentgenol 193:W244–W250. https://doi.org/10.2214/AJR.08.1838
17. De B, Kinnaman MD, Wexler LH et al (2018) Central nervous system relapse of rhabdomyosarcoma. Pediatr Blood Cancer. https://doi.org/10.1002/pbc.26710
18. Aerts I, Lumbroso-Le Rouic L, Gauthier-Villars M et al (2006) Retinoblastoma. Orphanet J Rare Dis 1:31. https://doi.org/10.1186/1750-1172-1-31
19. de Graaf P, Göricke S, Rodjan F et al (2012) Guidelines for imaging retinoblastoma: imaging principles and MRI standardization. Pediatr Radiol 42:2–14. https://doi.org/10.1007/s00247-011-2201-5
20. de Jong MC, Kors WA, de Graaf P et al (2014) Trilateral retinoblastoma: a systematic review and meta-analysis. Lancet Oncol 15:1157–1167. https://doi.org/10.1016/S1470-2045(14)70336-5
21. de Jong MC, Kors WA, de Graaf P et al (2015) The incidence of trilateral retinoblastoma: a systematic review and meta-analysis. Am J Ophthalmol 160:1116-1126.e5. https://doi.org/10.1016/j.ajo.2015.09.009
22. de Jong MC, Kors WA, Moll AC et al (2020) Screening for pineal trilateral retinoblastoma revisited: a meta-analysis. Ophthalmology 127:601–607. https://doi.org/10.1016/j.ophtha.2019.10.040
23. Galluzzi P, de Jong MC, Sirin S et al (2016) MRI-based assessment of the pineal gland in a large population of children aged 0–5 years and comparison with pineoblastoma: part I, the solid gland. Neuroradiology 58:705–712. https://doi.org/10.1007/s00234-016-1684-z
24. Sirin S, de Jong MC, Galluzzi P et al (2016) MRI-based assessment of the pineal gland in a large population of children aged 0–5 years and comparison with pineoblastoma: part II, the cystic gland. Neuroradiology 58:713–721. https://doi.org/10.1007/s00234-016-1683-0
25. Chung EM, Specht CS, Schroeder JW (2007) From the archives of the AFIP: pediatric orbit tumors and tumorlike lesions: neuroepithelial lesions of the ocular globe and optic nerve. Radiographics 27:1159–1186. https://doi.org/10.1148/rg.274075014
26. Jansen RW, de Bloeme CM, Brisse HJ et al (2020) MR imaging features to differentiate retinoblastoma from coats' disease and persistent fetal vasculature. Cancers (Basel). https://doi.org/10.3390/cancers12123592
27 Brisse HJ, European Retinoblastoma Imaging Collaboration (2010) Retinoblastoma Imaging. Ophthalmology 117:1051-1051.e1. https://doi.org/10.1016/j.ophtha.2009.12.022
28. Brisse HJ, de Graaf P, Galluzzi P et al (2015) Assessment of early-stage optic nerve invasion in retinoblastoma using high-resolution 1.5 Tesla MRI with surface coils: a multicentre, prospective accuracy study with histopathological correlation. Eur Radiol 25:1443–1452. https://doi.org/10.1007/s00330-014-3514-1
29. Sirin S, Schlamann M, Metz KA et al (2013) Diagnostic image quality of gadolinium-enhanced T1-weighted MRI with and without fat saturation in children with retinoblastoma. Pediatr Radiol 43:716–724. https://doi.org/10.1007/s00247-012-2576-y
30. Quirk B, Connor S (2020) Skull base imaging, anatomy, pathology and protocols. Pract Neurol 20:39–49. https://doi.org/10.1136/practneurol-2019-002383
31. Hudgins PA, Baugnon KL (2018) Head and neck: skull base imaging. Neurosurgery 82:255–267. https://doi.org/10.1093/neuros/nyx492
32. Muccio CF, Caranci F, D'Arco F et al (2014) Magnetic resonance features of pyogenic brain abscesses and differential diagnosis using morphological and functional imaging studies: a pictorial essay. J Neuroradiol 41:153–167. https://doi.org/10.1016/j.neurad.2014.05.004
33. Severino M, Liyanage S, Novelli V et al (2012) Skull base osteomyelitis and potential cerebrovascular complications in children. Pediatr Radiol 42:867–874. https://doi.org/10.1007/s00247-011-2340-8
34. Hoch BL, Nielsen GP, Liebsch NJ, Rosenberg AE (2006) Base of skull chordomas in children and adolescents: a clinicopathologic study of 73 cases. Am J Surg Pathol 30:811–818. https://doi.org/10.1097/01.pas.0000209828.39477.ab
35 Golden L, Pendharkar A, Fischbein N (2018) Imaging cranial base chordoma and chondrosarcoma. Chordomas and chondrosarcomas of the skull base and spine. Elsevier, pp 67–78

36. Talenti G, Picariello S, Robson C et al (2021) Magnetic resonance features and cranial nerve involvement in pediatric head and neck rhabdomyosarcomas. Neuroradiology 63:1925–1934. https://doi.org/10.1007/s00234-021-02765-0
37 Flors L, Leiva-Salinas C, Maged IM et al (2011) MR imaging of soft-tissue vascular malformations: diagnosis, classification, and therapy follow-up. Radiographics 31:1321–1340. https://doi.org/10.1148/rg.315105213
38. Mota EB, Penna CRR, Marchiori E (2017) Metastatic dissemination of a neuroblastoma. J Pediatr 189:232-232.e1. https://doi.org/10.1016/j.jpeds.2017.05.069
39. Purnell CA, Skladman R, Alden TD et al (2019) Nasal dermoid cysts with intracranial extension: avoiding coronal incision through midline exposure and nasal bone osteotomy. J Neurosurg Pediatr. https://doi.org/10.3171/2019.9.PEDS19132
40. Zaveri J, La Q, Yarmish G, Neuman J (2014) More than just Langerhans cell histiocytosis: a radiologic review of histiocytic disorders. Radiographics 34:2008–2024. https://doi.org/10.1148/rg.347130132
41. Weerakkody Y, Singh G (2005) Langerhans cell histiocytosis (skeletal manifestations). In: Radiopaedia.org. Radiopaedia.org
42. Chen H-C, Shen W-C, Chou D-Y, Chiang I-P (2002) Langerhans cell histiocytosis of the skull complicated with an epidural hematoma. AJNR Am J Neuroradiol 23:493–495
43. McClain KL, Picarsic J, Chakraborty R et al (2018) CNS Langerhans cell histiocytosis: common hematopoietic origin for LCH-associated neurodegeneration and mass lesions. Cancer 124:2607–2620. https://doi.org/10.1002/cncr.31348
44. Poe LB, Dubowy RL, Hochhauser L et al (1994) Demyelinating and gliotic cerebellar lesions in Langerhans cell histiocytosis. AJNR Am J Neuroradiol 15:1921–1928
45. Schäfer JF, Granata C, von Kalle T et al (2020) Whole-body magnetic resonance imaging in pediatric oncology - recommendations by the Oncology Task Force of the ESPR. Pediatr Radiol 50:1162–1174. https://doi.org/10.1007/s00247-020-04683-4
46. Godano E, Morana G, Di Iorgi N et al (2018) Role of MRI T2-DRIVE in the assessment of pituitary stalk abnormalities without gadolinium in pituitary diseases. Eur J Endocrinol 178:613–622. https://doi.org/10.1530/EJE-18-0094
47. Cerbone M, Visser J, Bulwer C et al (2021) Management of children and young people with idiopathic pituitary stalk thickening, central diabetes insipidus, or both: a national clinical practice consensus guideline. Lancet Child Adolesc Health 5:662–676. https://doi.org/10.1016/S2352-4642(21)00088-2
48. Meuwly J-Y, Lepori D, Theumann N et al (2005) Multimodality imaging evaluation of the pediatric neck: techniques and spectrum of findings. Radiographics 25:931–948. https://doi.org/10.1148/rg.254045142
49. Chiesa-Estomba CM, Ravanelli M, Farina D et al (2020) Imaging checklist for preoperative evaluation of laryngeal tumors to be treated by transoral microsurgery: guidelines from the European Laryngological Society. Eur Arch Otorhinolaryngol 277:1707–1714. https://doi.org/10.1007/s00405-020-05869-0
50. Elders BBLJ, Hermelijn SM, Tiddens HAWM et al (2019) Magnetic resonance imaging of the larynx in the pediatric population: a systematic review. Pediatr Pulmonol 54:478–486. https://doi.org/10.1002/ppul.24250
51. Maroldi R, Ravanelli M, Farina D (2014) Magnetic resonance for laryngeal cancer. Curr Opin Otolaryngol Head Neck Surg 22:131–139. https://doi.org/10.1097/MOO.0000000000000036
52. Ravanelli M, Farina D, Rizzardi P et al (2013) MR with surface coils in the follow-up after endoscopic laser resection for glottic squamous cell carcinoma: feasibility and diagnostic accuracy. Neuroradiology 55:225–232. https://doi.org/10.1007/s00234-012-1128-3
53. Avey G (2020) Technical improvements in head and neck MR imaging: at the cutting edge. Neuroimaging Clin N Am 30:295–309. https://doi.org/10.1016/j.nic.2020.04.002
54. Verbist BM (2012) Imaging of sensorineural hearing loss: a pattern-based approach to diseases of the inner ear and cerebellopontine angle. Insights Imaging 3:139–153. https://doi.org/10.1007/s13244-011-0134-z
55. Casselman JW, Offeciers EF, De Foer B et al (2001) CT and MR imaging of congential abnormalities of the inner ear and internal auditory canal. Eur J Radiol 40:94–104. https://doi.org/10.1016/s0720-048x(01)00377-1
56. Burd C, Pai I, Connor S (2020) Imaging anatomy of the retrotympanum: variants and their surgical implications. Br J Radiol 93:20190677. https://doi.org/10.1259/bjr.20190677
57. Joshi VM, Navlekar SK, Kishore GR et al (2012) CT and MR imaging of the inner ear and brain in children with congenital sensorineural hearing loss. Radiographics 32:683–698. https://doi.org/10.1148/rg.323115073
58. Quirk B, Youssef A, Ganau M, D'Arco F (2019) Radiological diagnosis of the inner ear malformations in children with sensorineural hearing loss. BJR Open 1:20180050. https://doi.org/10.1259/bjro.20180050
59. Talenti G, Manara R, Brotto D, D'Arco F (2018) High-resolution 3 T magnetic resonance findings in cochlear hypoplasias and incomplete partition anomalies: a pictorial essay. Br J Radiol 91:20180120. https://doi.org/10.1259/bjr.20180120
60. Finsterer J, Scorza FA, Fiorini AC, Scorza CA (2020) MEGDEL Syndrome. Pediatr Neurol 110:25–29. https://doi.org/10.1016/j.pediatrneurol.2020.03.009
61. Campion T, Taranath A, Pinelli L et al (2019) Imaging of temporal bone inflammations in children: a pictorial review. Neuroradiology 61:959–970. https://doi.org/10.1007/s00234-019-02258-1
62. Casselman JW, Kuhweide R, Deimling M et al (1993) Constructive interference in steady state-3DFT MR imaging of the inner ear and cerebellopontine angle. AJNR Am J Neuroradiol 14:47–57
63. Schmalbrock P, Brogan MA, Chakeres DW et al (1993) Optimization of submillimeter-resolution MR imaging methods for the inner ear. J Magn Reson Imaging 3:451–459. https://doi.org/10.1002/jmri.1880030304
64. Benson JC, Carlson ML, Lane JI (2020) MRI of the internal auditory canal, labyrinth, and middle ear: how we do it. Radiology 297:252–265. https://doi.org/10.1148/radiol.2020201767
65. Schwartz KM, Lane JI, Bolster BD, Neff BA (2011) The utility of diffusion-weighted imaging for cholesteatoma evaluation. AJNR Am J Neuroradiol 32:430–436. https://doi.org/10.3174/ajnr.A2129
66. Dudau C, Draper A, Gkagkanasiou M et al (2019) Cholesteatoma: multishot echo-planar vs non echo-planar diffusion-weighted MRI for the prediction of middle ear and mastoid cholesteatoma. BJR Open 1:20180015. https://doi.org/10.1259/bjro.20180015
67. De Foer B, Vercruysse J-P, Bernaerts A et al (2007) The value of single-shot turbo spin-echo diffusion-weighted MR imaging in the detection of middle ear cholesteatoma. Neuroradiology 49:841–848. https://doi.org/10.1007/s00234-007-0268-3
68. Wiesmueller M, Wuest W, May MS et al (2021) Comparison of readout-segmented echo-planar imaging and single-shot TSE DWI for cholesteatoma diagnostics. AJNR Am J Neuroradiol 42:1305–1312. https://doi.org/10.3174/ajnr.A7112
69. Lingam RK, Nash R, Majithia A et al (2016) Non-echoplanar diffusion weighted imaging in the detection of post-operative middle ear cholesteatoma: navigating beyond the pitfalls to find the pearl. Insights Imaging 7:669–678. https://doi.org/10.1007/s13244-016-0516-3

70. Lingam RK, Bassett P (2017) A meta-analysis on the diagnostic performance of non-echoplanar diffusion-weighted imaging in detecting middle ear cholesteatoma: 10 years on. Otol Neurotol 38:521–528. https://doi.org/10.1097/MAO.0000000000001353
71. Nash R, Wong PY, Kalan A et al (2015) Comparing diffusion weighted MRI in the detection of post-operative middle ear cholesteatoma in children and adults. Int J Pediatr Otorhinolaryngol 79:2281–2285. https://doi.org/10.1016/j.ijporl.2015.10.025
72. De Foer B, Vercruysse J-P, Bernaerts A et al (2010) Middle ear cholesteatoma: non-echo-planar diffusion-weighted MR imaging versus delayed gadolinium-enhanced T1-weighted MR imaging–value in detection. Radiology 255:866–872. https://doi.org/10.1148/radiol.10091140
73. De Foer B, Vercruysse JP, Spaepen M et al (2010) Diffusion-weighted magnetic resonance imaging of the temporal bone. Neuroradiology 52:785–807. https://doi.org/10.1007/s00234-010-0742-1
74. Kanona H, Stephenson K, D'Arco F et al (2018) Computed tomography versus magnetic resonance imaging in paediatric cochlear implant assessment: a pilot study and our experience at Great Ormond Street Hospital. J Laryngol Otol 132:529–533. https://doi.org/10.1017/S0022215118000440
75. D'Arco F, Youssef A, Ioannidou E et al (2020) Temporal bone and intracranial abnormalities in syndromic causes of hearing loss: an updated guide. Eur J Radiol 123:108803. https://doi.org/10.1016/j.ejrad.2019.108803
76. Connor SEJ, Borri M, Pai I, Barnsley H (2021) "Black Bone" magnetic resonance imaging as a novel technique to aid the pre-operative planning of posterior tympanotomy for cochlear implantation. Cochlear Implants Int 22:35–41. https://doi.org/10.1080/14670100.2020.1823126
77. Yuhasz M, Hoch MJ, Hagiwara M et al (2018) Accelerated internal auditory canal screening magnetic resonance imaging protocol with compressed sensing 3-dimensional T2-weighted sequence. Invest Radiol 53:742–747. https://doi.org/10.1097/RLI.0000000000000499
78. Srinivasan R, So CW, Amin N et al (2019) A review of the safety of MRI in cochlear implant patients with retained magnets. Clin Radiol 74:972.e9-972.e16. https://doi.org/10.1016/j.crad.2019.06.011
79. Lu W, Pauly KB, Gold GE et al (2009) SEMAC: slice encoding for metal artifact correction in MRI. Magn Reson Med 62:66–76. https://doi.org/10.1002/mrm.21967
80. Amin N, Pai I, Touska P, Connor SEJ (2021) Utilization of SEMAC-VAT MRI for improved visualization of posterior fossa structures in patients with cochlear implants. Otol Neurotol 42:e451–e458. https://doi.org/10.1097/MAO.0000000000003016
81 Sharma D, Sharma N, Sharma V (2019) Sinonasal cancers: diagnosis and management. In: Wang T-C (ed) Challenging issues on paranasal sinuses. IntechOpen
82. Sen S, Chandra A, Mukhopadhyay S, Ghosh P (2015) Imaging approach to sinonasal neoplasms. Neuroimaging Clin N Am 25:577–593. https://doi.org/10.1016/j.nic.2015.07.005
83. Kushchayeva YS, Kushchayev SV, Glushko TY et al (2018) Fibrous dysplasia for radiologists: beyond ground glass bone matrix. Insights Imaging 9:1035–1056. https://doi.org/10.1007/s13244-018-0666-6
84. O'Brien WT, Hamelin S, Weitzel EK (2016) The preoperative sinus CT: avoiding a "CLOSE" call with surgical complications. Radiology 281:10–21. https://doi.org/10.1148/radiol.2016152230
85. Mossa-Basha M, Blitz AM (2013) Imaging of the paranasal sinuses. Semin Roentgenol 48:14–34. https://doi.org/10.1053/j.ro.2012.09.006
86. Som PM, Curtin HD (1994) Inflammatory lesions and tumors of the nasal cavities and paranasal sinuses with skull base involvement. Neuroimaging Clin N Am 4:499–513
87. Loevner LA, Sonners AI (2002) Imaging of neoplasms of the paranasal sinuses. Magn Reson Imaging Clin N Am 10:467–493. https://doi.org/10.1016/s1064-9689(02)00006-5
88. Madani G, Beale TJ, Lund VJ (2009) Imaging of sinonasal tumors. Semin Ultrasound CT MR 30:25–38. https://doi.org/10.1053/j.sult.2008.10.013
89. Eisen MD, Yousem DM, Montone KT et al (1996) Use of preoperative MR to predict dural, perineural, and venous sinus invasion of skull base tumors. AJNR Am J Neuroradiol 17:1937–1945
90. Farina D, Borghesi A, Botturi E et al (2010) Treatment monitoring of paranasal sinus tumors by magnetic resonance imaging. Cancer Imaging 10:183–193. https://doi.org/10.1102/1470-7330.2010.0025
91. Maroldi R, Ravanelli M, Farina D et al (2015) Post-treatment evaluation of paranasal sinuses after treatment of sinonasal neoplasms. Neuroimaging Clin N Am 25:667–685. https://doi.org/10.1016/j.nic.2015.07.009
92 Ho M-L (2021) Advanced pediatric neuroimaging: "better, stronger, faster." Magn Reson Imaging Clin N Am 29:xvii–xviii. https://doi.org/10.1016/j.mric.2021.07.001
93. Kirsch CF, Ho M-L (2021) Advanced magnetic resonance imaging of the skull base. Semin Ultrasound CT MR 42:229–252. https://doi.org/10.1053/j.sult.2021.04.006
94. Lu A, Gorny KR, Ho ML (2019) Zero TE MRI for craniofacial bone imaging. AJNR Am J Neuroradiol 40:1562–1566. https://doi.org/10.3174/ajnr.A6175
95. Kobayashi N, Bambach S, Ho M-L (2021) Ultrashort echo-time MR imaging of the pediatric head and neck. Magn Reson Imaging Clin N Am 29:583–593. https://doi.org/10.1016/j.mric.2021.06.008
96. Nanjappa M, Kolipaka A (2021) Magnetic resonance elastography of the brain. Magn Reson Imaging Clin N Am 29:617–630. https://doi.org/10.1016/j.mric.2021.06.011
97. Yeung DKW, Bhatia KS, Lee YYP et al (2013) MR elastography of the head and neck: driver design and initial results. Magn Reson Imaging 31:624–629. https://doi.org/10.1016/j.mri.2012.09.008
98. Deelchand DK, Ho M-L, Nestrasil I (2021) Ultra-high-field imaging of the pediatric brain and spinal cord. Magn Reson Imaging Clin N Am 29:643–653. https://doi.org/10.1016/j.mric.2021.06.013
99. van Egmond SL, Visser F, Pameijer FA, Grolman W (2014) Ex vivo and in vivo imaging of the inner ear at 7 Tesla MRI. Otol Neurotol 35:725–729. https://doi.org/10.1097/MAO.0000000000000276
100. Prabhu SP (2021) 3D modeling and advanced visualization of the pediatric brain, neck, and spine. Magn Reson Imaging Clin N Am 29:655–666. https://doi.org/10.1016/j.mric.2021.06.014
101. Eley KA, Rossi-Espagnet MC, Schievano S et al (2021) Multiparametric imaging for presurgical planning of craniopagus twins: the experience of two tertiary pediatric hospitals with six sets of twins. Radiology 298:18–27. https://doi.org/10.1148/radiol.2020202216
102. Mamlouk MD, Hess CP (2016) Arterial spin-labeled perfusion for vascular anomalies in the pediatric head and neck. Clin Imaging 40:1040–1046. https://doi.org/10.1016/j.clinimag.2016.06.009
103. Mossa-Basha M, Zhu C, Wu L (2021) Vessel wall MR imaging in the pediatric head and neck. Magn Reson Imaging Clin N Am 29:595–604. https://doi.org/10.1016/j.mric.2021.06.009
104. Fujima N, Carlota Andreu-Arasa V, Barest GD et al (2020) Magnetic resonance spectroscopy of the head and neck: principles,

applications, and challenges. Neuroimaging Clin N Am 30:283–293. https://doi.org/10.1016/j.nic.2020.04.006
105. Jones KM, Pollard AC, Pagel MD (2018) Clinical applications of chemical exchange saturation transfer (CEST) MRI. J Magn Reson Imaging 47:11–27. https://doi.org/10.1002/jmri.25838
106. Pareek A, Muehe AM, Theruvath AJ et al (2017) Whole-body PET/MRI of pediatric patients: the details that matter. J Vis Exp. https://doi.org/10.3791/57128
107. Sepehrizadeh T, Jong I, DeVeer M, Malhotra A (2021) PET/MRI in paediatric disease. Eur J Radiol 144:109987. https://doi.org/10.1016/j.ejrad.2021.109987